Magnification and resolution of microlenses with different shapes

Jinglei Hou[1,2], Ling Yao[1,2], Jie Ren[1,2], Minglei Guo[1,2], Yong-Hong Ye[1,2]

[1]*School of Physics and Technology, Nanjing Normal University, Nanjing 210023, People's Republic of China*
[2]*Jiangsu Provincial Key Laboratory of Optoelectronic Technology, Nanjing Normal University, Nanjing 210023, People's Republic of China*
E-mail: yeyonghong@njnu.edu.cn

Published in Micro & Nano Letters; Received on 4th March 2015; Revised on 21st April 2015; Accepted on 22nd April 2015

In this reported work, three types of microlenses, the whole microsphere solid lens (W-SL), the melted microsphere solid lens (M-SL) and the microsphere solid lens semi-immersed in SU-8 resist (S-SL), have been fabricated from mircospheres with a diameter of 2.87 μm. Their imaging properties on the nanosphere arrays with diameters of 280–600 nm were experimentally studied. It was found that the shape of the microlens plays an important role in the imaging properties. The imaging resolution of the S-SL is the best as more high Fourier components of the object can be coupled into the lens, while the magnification (~2.0×) of the M-SL is the largest.

1. Introduction: Optical microscopes are the most commonly used imaging tools. However, an object of 300–400 nm is difficult to be observed under an optical microscope, because of the limitation of the Abbe diffraction limit. To observe smaller objects, non-lens based approaches have been developed, such as scanning electron microscopy (SEM), atomic force microscopy (AFM), scanning near-field optical microscopy (SNOM) and so on. Recently, researchers have observed that super resolution imaging can be obtained by spherical microlenses [1–17]. The features of microlenses for magnifying and resolving nano-objects have also been studied [4–16]. A TiO_2 colloid with a diameter of 2 μm has been successfully used for single molecule imaging [13]. Near-field infrared imaging with a micro-fabricated solid immersion lens has been studied [11]. Near-field focusing and magnification through nanoscale hemispherical lenses have been studied by Lee *et al.* [14] Wang *et al.* [8] have experimentally demonstrated that silica microspheres with diameters in the range of 2–9 μm can observe the stripes of a blu-ray disc with a traditional optical microscope. The magnified virtual image has a sharper contrast when the microscale spherical lens is semi-immersed in liquid as has been demonstrated by Hao *et al.* [16]. Lee *et al.* [18] have also reported that larger PS microspheres of 30, 50 and 100 μm can overcome the diffraction limit in optical imaging. Vlad *et al.* [19] have discovered that the magnification and field of view (FOV) can be affected by the shape of the microlens. However, how the shape of the microlens affects the FOV, magnification and resolution of whole microsphere solid lens (W-SL), the melted microsphere solid lens (M-SL), and the M-SL semi-immersed in SU-8 resist (S-SL) have not been studied systematically.

In this Letter, we study the imaging properties of different-shaped microlenses. The three microlenses studied are the W-SL, M-SL and microsphere solid lens S-SL. We find that the W-SL cannot resolve 280–600 nm nanosphere arrays. The magnification of the M-SL is the largest among these three microlenses, about 2.0×. Moreover, the image resolution of the S-SL is the best among these three microlenses. We consider that the lager numerical aperture (NA) of the S-SL plays an important role in its high image resolution. The FOV also depends on the shape of the microlenses.

2. Experimental procedure: The schematic of the experimental setup is shown in Fig. 1*a*. Self-assembled polystyrene (PS) microsphere arrays were used as the image objects (samples). The diameters of the microspheres used in this experiment are 280, 305, 400 nm and 600 nm, respectively. The detailed fabrication process of these samples was described in one of our previous publications [20]. The samples were put under a Leica microscope, and the reflected images of the PS microsphere arrays though a wavelength microscale lens with different shapes were observed and recorded by a 100 × (NA = 0.9) microscope objective with a charge-coupled device camera with the pixel number of 2048 × 1536. The Rayleigh resolution limit for point objects is 366 nm ($r = 0.61\,\lambda$/nNA); here $\lambda = 540$ nm, $n = 1$, and NA = 0.9 [21]. When a SU-8 layer is coated on top of the objects, the Rayleigh resolution limit can be calculated as $0.61\,\lambda$/nNA = 229 nm for point objects; $n = 1.6$ is the refractive index of the SU-8. Therefore, the four kinds of objects (280, 305, 400 and 600 nm) observed are all beyond the Rayleigh resolution limit when we used the S-SL. Fig. 1*b* shows the SEM image of a type of self-assembled PS microsphere array. The diameter of the PS microsphere was 305 nm in this sample. As shown in Fig. 1*b*, the microspheres are hexagonally close-packed. The detailed fabrication procedure of the substrates can be found in [22].

Fig. 2 shows the SEM images of the three different microlenses. As shown in Fig. 2*a*, the diameter of the W-SL is 2.87 μm. Fig. 2*b* is the image of the M-SL. This microlens was obtained when a 2.87 μm PS microsphere was melted for 30 min on a hot plate. The SEM image of the S-SL is shown in Fig. 2*c*. Its detailed fabrication process can be also found in [20]. To study the optical imaging properties of the three microlenses with different shapes we used them to observe the objects fabricated with different sized microspheres.

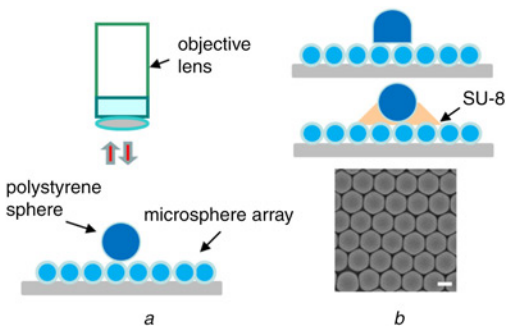

Figure 1 *Schematic representation of experimental setup*
a Schematic of experimental setup
b SEM image of a self-assembled PS microsphere array; diameter of microsphere is 305 nm
Scale bar is 200 nm

© The Institution of Engineering and Technology 2015

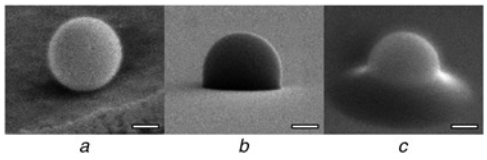

Figure 2 *SEM images of the three microslenses with different shapes*
a W-SL
b M-SL
c S-SL
Scale bar is 1 μm

3. Results and discussion: Figs. 3*a–c* exhibit the images observed by the three microlenses of an object fabricated with 280 nm microspheres while Figs. 3*d–f* are the images of an object fabricated with 305 nm microspheres. Figs. 3*a* and *d* show that there are no images observed by the W-SL. Figs. 3*b* and *e* illustrate that the images are quite blurred when observed by the M-SL; the image in Fig. 3*e* is a little clearer than the one in Fig. 3*b*. Figs. 3*c* and *f* indicate that the image observed by the S-SL is sharper and obvious. The magnification factor M of the two objects are ∼1.64×. Obviously, the number of microspheres of the images in Figs. 3*b* and *e* is less than that in Figs. 3*c* and *f*. The resolution and FOV of the S-SL is much larger than that of the M-SL. As shown in Figs. 3*b–f*, the obtained resolution and FOV strongly depend on the morphology of the microlenses. Because the virtual images in Figs. 3*b* and *e* are not clear, the magnification cannot be calculated. To obtain a more in-depth study on the magnification and resolution, we used these different three microlenses to observe another two larger objects.

Fig. 4 shows optical images of the three different microlenses on an object fabricated with 400 nm microspheres. There is also no image observed by the W-SL, as shown in Fig. 4*a*. However, Fig. 4*b* shows that a virtual image can be clearly observed by the M-SL and M is ∼2.01×. As shown in Fig. 4*c*, two virtual images are formed, image (c_1) which is clear and image (c_2) which is blurring; M is ∼1.83× and ∼2.86× for the clear and blurring images, respectively.

To further analyse the imaging behaviours of the three different microlenses, their imaging properties on a larger object are also studied. Fig. 5 displays images of the three microlenses on a sample fabricated with 600 nm microspheres. Fig. 5*a* shows no virtual image observed by the W-SL, while a very blurring real image is formed above the W-SL. Fig. 5*b* indicates that the

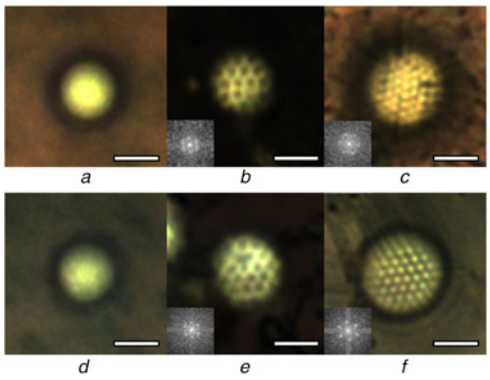

Figure 3 *Optical images of the three microlenses with different shapes on two objects*
a, *d* Optical images of the W-SL
b, *e* Optical images of the M-SL
c, *f* Optical images of the S-SL
a–c The objects we observed were fabricated from 280 nm PS microspheres
d–f The objects we observed were fabricated from 305 nm PS microspheres.
Scale bar is 2 μm

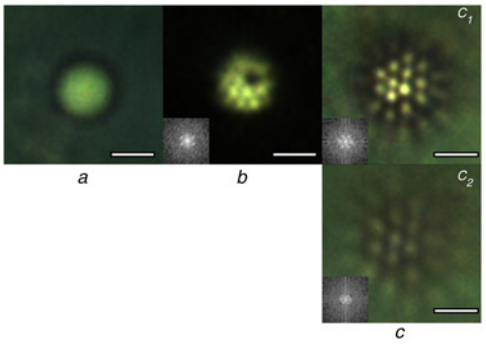

Figure 4 *Optical images of the three microlenses with different shapes on object fabricated from 400 nm microspheres*
a Optical image of the W-SL
b Optical image of the M-SL
c Optical images of the S-SL and two virtual images are formed
Scale bar is 2 μm

virtual image is clearly observed by the M-SL, M being ∼1.93×. Fig. 5*c* shows that there are also two virtual images formed (image (c_1) is clear and image (c_2) is blurring), M being ∼1.72× and ∼2.65× for the clear image and the blurring image, respectively. The relative experimental results are summarised in Table 1.

Our experimental results indicate the following. (i) All these different sized microspheres (280–600 nm) cannot be resolved by the W-SL. (ii) For the M-SL, the object cannot be observed clearly until its size is 400 nm, and the magnification is the largest. (iii) Different sizes of microspheres with the range of 280–600 nm can all be resolved by the S-SL and the image is clear and bright. (iv) The resolution and FOV of the S-SL is both the best and the largest.

To analyse these results, the frequency spectra of the images in Figs. 3–5 were calculated by Fourier analysis, and are also shown in the insets of the Figures. The low-frequencies located at the centre and the high-frequencies at the corners. The frequency spectra of the images through the M-SL show that they mainly have small lateral wave vector Fourier components. The situations of the S-SL are complex. The frequency spectra of optical images of the S-SL on a small object indicate that they mainly have large lateral wave vector components. And the frequency spectra of the big objects' images also show that the blurred images have a very large proportion of small lateral wave vector components, while the clear images have more large lateral wave vector components than the blurred images. The resolution of the S-SL is best although its experimental magnification becomes smaller than the M-SL's. We propose that the resolution of the S-SL is high, because the

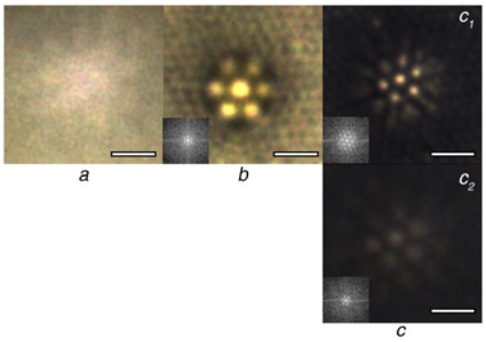

Figure 5 *Optical images of the three microlenses with different shapes on object fabricated with 600 nm microspheres*
a Optical image of the W-SL
b Optical image of the M-SL
c Optical images of the S-SL and two virtual images are formed
Scale bar is 2 μm

© The Institution of Engineering and Technology 2015

doi: 10.1049/mnl.2015.0082

Table 1 Experimental magnification of the images

Microspheres, nm	M-SL		S-SL	
	Clear images	Blurred images	Clear images	Blurred images
280	none	none	1.64×	none
305	none	none	1.64×	none
400	2.01×	none	1.83×	2.86×
600	1.93×	none	1.72×	2.65×

more large lateral wave vector enters into the S-SL. In a previous study [19], the conclusion is that the imaging property of the half melted micolens is best among the whole microlens and other microlenses which are obtained from different melting times. Our experimental results indicate that the imaging resolution property of the S-SL is best among these three different microlens (W-SL, M-SL, S-SL).

The focal plane of the object space from the centre of the microlenses (F) of these microlenses is calculated by computer simulation technology (CST). CST is a commercial finite-different time-domain program that can achieve the exact solution of the Maxwell's equation. Studies have also shown that the calculation results obtained from CST conform to the actual situation [20, 23]. F of the M-SL obtained from CST is 1.01 μm. The magnification is ∼1.86×. It is obtained by using the paraxial ray-tracing formulae, $M = f/(f + l)$, where f is the focal length of the microlens, and l is the length between the centre of the micolens and the object. When the microlens is close to the samples, l is equal to $-d/2$ (d is the diameter of the microlens).

We think it is that the terajet promotes the resolution of the M-SL [24]. However, the S-SL has two F calculated by CST. The shorter one is 2.21 μm, the other is 6.73 μm. The calculated magnification is ∼2.85× and ∼1.27×, respectively. Based on the calculated magnification, it can also be seen that the experimental M of the M-SL matches well with the magnification calculated by using F obtained from CST. Moreover, the magnification of the clear images observed by the S-SL does not match with the magnification calculated by the geometrical optics, therefore we consider that it is that super resolution works (large lateral wave vector components). Our previous studies have demonstrated that experimental magnification of the blurring images observed by the S-SL is very close to the calculated magnification [20].

The super resolution performance of the S-SL is remarkable, and the FOV of the S-SL is the largest among these three microlenses. The dotted red lines in Fig. 6 represent the objective aperture angle. θ_a, θ_b and θ_c are half of their objective aperture angle. It is well known that the Rayleigh resolution limit for the point objects is r ($r = 0.61\,\lambda/\mathrm{nNA}$), $\mathrm{NA} = n \times \sin\alpha$, n is the refractive index of the medium, and α is half of the objective aperture angle. The larger the NA, the higher is the image resolution. In our experiment, n is 1, 1 and 1.6 for the W-SL, M-SL and S-SL, and $\theta_a < \theta_b < \theta_c$, $\mathrm{NA}_a < \mathrm{NA}_b < \mathrm{NA}_c$, and the calculated results indicate that $r_{\text{W-SL}} > r_{\text{M-SL}} > r_{\text{S-SL}}$. Therefore, the resolution of the S-SL is the highest among the three microlenses. The dotted black curves in Fig. 6 demonstrate the FOV of the microlenses. They indicate that the interface area between a W-SL and a sample is the smallest among the three lenses, hence the FOV of the W-SL is also smallest. The smaller is that of the M-SL, and the FOV of the S-SL is the largest. By analysing the wave vector propagation as shown in Fig. 6, we can find that the larger the interface area, the more wave vectors can enter into the microlens. We propose that a large FOV of the S-SL plays a positive role in improving its resolution. Few microspheres' information waves can be coupled into the W-SL, which can explain why microspheres with diameters between 280–600 nm cannot be observed by the W-SL. In addition,

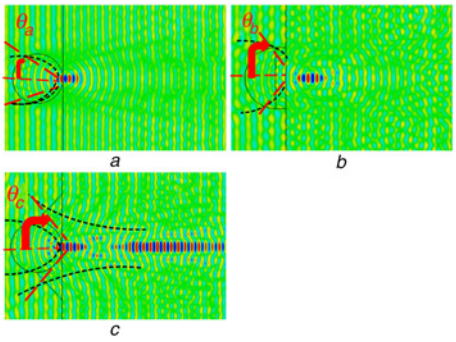

Figure 6 *CST simulation results*
a–c Light propagation of the three microlenses
a W-SL
b M-SL
c S-SL
$\lambda = 540$ nm

by studying the magnification and F calculated by CST, we can find that the closer the distance between the microlens and the object, the greater the magnification. We believe that the larger magnification of the M-SL is associated with this theory.

4. Conclusion: In summary, the resolution of the S-SL is the best among the three microlenses, although the M is smaller than that of the M-SL. We have demonstrated that the FOV of the S-SL is largest among the microlenses. By investigating the properties of these microlenses we find that the property of the S-SL is the best in the micro optical imaging field among these three microlenses. The shape of the S-SL plays an important role in the super resolution.

5. Acknowledgments: This work was supported by the Doctoral Fund of Ministry of Education of China (grant no. 20133207110007) and by the National Natural Science Foundation of China (grant no. 61475073).

6 References

[1] Fang N., Lee H., Sun C., Zhang X.: 'Sub-diffraction-limited optical imaging with a silver superlens', *Science*, 2013, **308**, (5721), pp. 534–537
[2] Pendry J.B.: 'Negative refraction makes a perfect lens', *Phys. Rev. Lett.*, 2000, **85**, (18), pp. 3966–3969
[3] Zhang X., Liu Z.: 'Superlenses to overcome the diffraction limit', *Nat. Materials*, 2008, **7**, pp. 435–441
[4] Hell S.W., Schmidt R., Egner A.: 'Diffraction-unlimited three-dimensional optical nanoscopy with opposing lenses', *Nat. Photonics*, 2009, **3**, pp. 381–387
[5] Kawata S., Inouye Y., Verma P.: 'Plasmonics for near-field nano-imaging and superlensing', *Nat. Photonics*, 2009, **3**, pp. 388–394
[6] Rho J., Ye Z., Xiong Y., *ET AL.*: 'Spherical hyperlens for two-dimensional sub-diffractional imaging at visible frequencies', *Nat. Commun.*, 2010, **1**, p. 1148
[7] Van Putten E.G., Akbulut D., Bertolotti J., Vos W.L., Lagendijk A., Mosk A.P.: 'Scattering lens resolves sub-100 nm structures with visible light', *Phys. Rev. Lett.*, 2011, **106**, p. 193905
[8] Wang Z., Guo W., Li L., *ET AL.*: 'Optical virtual imaging at 50 nm lateral resolution with a white-light nanoscope', *Nat. Commun., March*, 2011, **2**, doi: 10.1038/ncomms1211
[9] Lu D., Liu Z.: 'Hyperlenses and metalenses for far-field super-resolution imaging', *Nat. Commun.*, 2012, **3**, doi: 10.1038/ncomms2176
[10] Lemoult F., Fink M., Lerosey G.: 'A polychromatic approach to far-field superlensing at visible wavelengths', *Nat. Commun.*, 2012, **3**, doi: 10.1038/ncomms1885
[11] Fletcher D.A., Crozier K.B., Quate C.F., *ET AL.*: 'Near-field infrared imaging with a microfabricated solid immersion lens', *Appl. Phys. Lett.*, 2000, **77**, (14), pp. 2109–2111

© The Institution of Engineering and Technology 2015

[12] Wenger J., Gerard D., Aouani H., Rigneault H.: 'Disposable microscope objective lenses for fluorescence correlation spectroscopy using latex microspheres', *Anal. Chem.*, 2000, **80**, (17), pp. 6800–6804
[13] Schwartz J.J., Stavrakis S., Quake S.R.: 'Colloidal lenses allow high-temperature single-molecule imaging and improve fluorophore photostability', *Nat. Nanotechnology*, 2010, **5**, (2), pp. 127–132
[14] Lee J.Y., Hong B.H., Kim W.Y., *ET AL.*: 'Near-field focusing and magnification through self-assembled nanoscale spherical lenses', *Nature*, 2009, **460**, (7254), pp. 498–501
[15] Rogers E., Lindberg J., Roy T., *ET AL.*: 'A super-oscillatory lens optical microscope for subwavelength imaging', *Nat. Materials*, 2012, **11**, pp. 432–435
[16] Hao X., Kuang C., Liu X., Zhang H., Li Y.: 'Microsphere based microscope with optical super-resolution capability', *Appl. Phys. Lett.*, 2011, **99**, (20), p. 203102
[17] Darafsheh A., Walsh G.F., Negro L.D., Astratov V.N.: 'Optical super-resolution by high-index liquid-immersed microspheres', *Appl. Phys. Lett.*, 2012, **101**, (14), p. 141128
[18] Lee S., Li L., Aryeh Y.B., Wang Z., Guo W.: 'Overcoming the diffraction limit induced by microsphere optical nanoscopy', *J. Opt.*, 2013, **15**, (12), p. 125710
[19] Vlad A., Huynen I., Melinte S.: 'Wavelength-scale lens microscopy via thermal reshaping of colloidal particles', *Nanotechnology*, 2012, **23**, (28), p. 285708
[20] Ye R., Ye Y., Ma H.F., *ET AL.*: 'Experimental imaging properties of immersion microscale spherical lenses', *Sci. Rep.*, 2014, **4**, doi: 10.1038/srep03769
[21] Goldstein D.J.: 'A quantitative computer simulation of microscopic imaging', *J. Microsc.*, 1991, **162**, (2), pp. 241–253
[22] Ye Y., LeBlanc F., Hache A., Truong V.: 'Self-assembling three-dimensional colloidal photonic crystal structure with high crystalline quality', *Appl. Phys. Lett.*, 2001, **78**, (1), pp. 52–54
[23] Ran Y., Ye Y., Ma H.F., *ET AL.*: 'Experimental far-field imaging properties of a ∼5-μm diameter spherical lens', *Opt. Let.*, 2013, **38**, (11), pp. 1829–1831
[24] Pacheco-pena V., Beruete M., Minin I.V., Minin O.V.: 'Multifrequency focusing and wide angular scanning of terajets', *Opt. Let.*, 2015, **40**, (2), pp. 245–248

© The Institution of Engineering and Technology 2015

doi: 10.1049/mnl.2015.0082